Electronic and electrostatic properties of polar oxide nanostructures: MgO(111) islands on Au(111)

Niklas Nilius,[1,*] Stefania Benedetti,[2] Yi Pan,[1] Philipp Myrach,[1] Claudine Noguera,[3] Livia Giordano,[4] and Jacek Goniakowski[3,*]

[1]*Fritz-Haber-Institut der Max-Planck-Gesellschaft, Faradayweg 4-6, D-14195 Berlin, Germany*

[2]*Centro S3, Instituto Nanoscienze-CNR, via Campi 213/a, 41125 Modena, Italy*

[3]*CNRS and Université Pierre et Marie Curie-Paris 6, INSP, UMR7588, 4 place Jussieu, 75252 Paris, Cedex 05, France*

[4]*Dipartimento di Scienza dei Materiali, Università di Milano-Bicocca, via Cozzi 53, 20125 Milano, Italy*

(Received 7 August 2012; revised manuscript received 15 October 2012; published 6 November 2012)

Using scanning tunneling microscopy and density functional theory (DFT), we have analyzed the local electronic properties of (111)-oriented MgO nanoislands on Au(111). Conductance and barrier-height measurements revealed substantial modulations in the electronic structure and electrostatic potential across the islands, with particularly high and low values for band onsets and surface potential occurring at the perimeter and in the island center, respectively. DFT calculations showed that MgO(111) monolayer structures exhibit a strongly reduced distance between the $Mg^{\delta+}$ and $O^{\delta-}$ plane as compared to bulk MgO, which in turn suppresses the polar character of the film. The spatial modulations in the electronic properties originate from gradual changes of the interface registry when approaching the island edges, driven by a small mismatch between the Au(111) and MgO(111) lattices. At the periphery of the islands, additional effects such as band shifts and low-lying electronic states are observed, which arise from the interplay of residual edge polarity and unsaturated chemical bonds. We expect that the peculiar edge properties of MgO(111) islands are decisive for the chemical behavior of the nanostructures.

DOI: 10.1103/PhysRevB.86.205410 PACS number(s): 73.61.Ng, 68.55.aj, 77.22.Ej, 68.37.Ef

I. INTRODUCTION

The polar nature of ionic nanoobjects attracts increasing attention in the surface science community.[1] Metal-supported ultrathin oxide films that comprise only a few atomic layers grown along a polar direction were shown to display a variety of unusual properties.[2–5] The observation of unreconstructed MgO(111)/Ag(111),[6] FeO(111)/Pt(111),[7–9] and ZnO/Pd(111) films[10] suggests the existence of polarity-compensation mechanisms that differ from those known for bulk oxides. Indeed, while at polar surfaces of bulk materials, a diverging electrostatic potential is suppressed by a thorough modification of the surface charge density,[1] thin polar films may sustain a substantial dipole moment and exist in an uncompensated polar state with specific, thickness-dependent properties.[11] Alternatively, polar instabilities may induce a complete restructuring of the films, resulting in lattice geometries that are unstable in the bulk limit. For example, the polarity-driven formation of boron-nitride (B_k) structures with cations and anions lying in the same (0001) plane has been revealed, theoretically and experimentally, for MgO(111),[6,12] ZnO(0001),[13] and CoO(111) films.[14] Calculations for unsupported MgO(111),[12] FeO(111),[15] and ZnO(0001)[16] monolayers even demonstrated that such systems are always nonpolar, as the distance between oppositely charged ion planes vanishes.

In presence of a conductive substrate, the character of ultrathin films is further modified by covalent and electrostatic interactions at the interface. In particular, a polarization (rumpling) of the oxide lattice occurs in response to an interfacial charge transfer between ad-layer and metal support.[17,18] This phenomenon, termed induced polarity, is present in ultrathin films of both polar and nonpolar termination and heavily affects their electronic properties and work function. For MgO grown on an electronegative substrate, such as gold, the induced polarization gives rise to an outward relaxation of the O-anions, which increases the work function and hence opposes the trend set by the charge transfer and the modified electronic structure at the interface.[19–21] Since those effects are very sensitive to the local interface structure, any change in the atomic registry between oxide film and metal support, for instance due to an imperfect lattice match, substantially alters the electrostatic potential and electronic structure of the thin-film system. Such variations have indeed been observed for nonpolar MgO/Mo(001)[22,23] and polar FeO/Pt(111) films,[15,24] where regular work function patterns having the periodicity of the metal-oxide coincidence lattice were found.

Beyond the classical polarity effects recalled before, additional electrostatic instabilities might be induced by polar edges, as present in many spatially confined ionic systems.[25,26] We have recently demonstrated how in-plane polarity influences the relative stability of supported MgO islands and promotes the growth of square-lattice MgO(001) on supports with hexagonal lattice symmetry, such as Au(111).[27] However, little is known on the local electronic structure of such polar terminations, in particular on the charge redistribution, the local surface potential, and the band onsets in presence of a finite in-plane dipole moment.

In this paper, scanning tunneling microscopy (STM) and density functional theory (DFT) were combined to elucidate the electronic properties of (111)-oriented MgO islands grown on an Au(111) support. STM conductance and barrier-height measurements identified unusual electronic properties at the island periphery as compared to the inner regions, being explained with a change of the lattice registry at the metal-oxide interface. DFT calculations revealed a reduced distance between cationic and anionic oxide planes, validating the concept of induced polarity introduced previously. The polar nature of the island edges, on the other hand, seems to be less important for the observed structural and electronic characteristics.

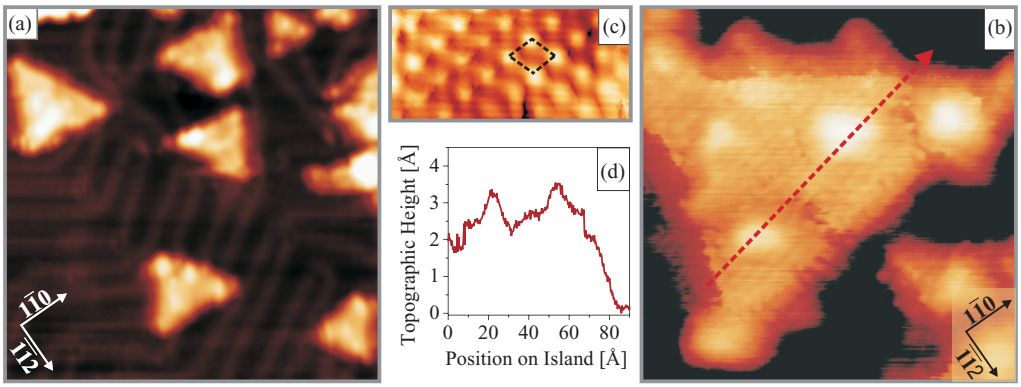

FIG. 1. (Color online) (a) Overview ($V_s = -0.5$ V, 400×400 Å^2), (b) close-up (0.05 V, 90×90 Å^2), and (c) atomically resolved STM image (0.05 V, 25×10 Å^2) of triangular MgO islands on Au(111). (d) Height profile taken along the dashed line in (b).

II. EXPERIMENT AND THEORY

The experiments were carried out in an ultrahigh-vacuum STM operated at 4.5 K. Imaging of the sample was performed in the constant current mode, while electronic properties were derived from conductance spectroscopy performed with lock-in technique. Information on the local surface potential was acquired from effective barrier-height (Φ_{eff}) measurements, probing the tunnel barrier, the electrons have to overcome when entering the sample. The Φ_{eff} value is derived from the current response to periodic modulations of the tip height ($\Delta z = 1$ Å) according to $\Phi_{\text{eff}} \propto \frac{\hbar^2}{8m}(\frac{d \ln I}{dz})^2$.[28] Note that Φ_{eff} is a monotonous function of, but not identical with, the true work function Φ.[29] The oxide islands were prepared by depositing 0.5 monolayer (ML) Mg in 1×10^{-6} mbar O_2 onto a sputtered/annealed Au(111) surface at room temperature.[21] The H_2O partial pressure was kept below 1×10^{-9} mbar during preparation, and the sample was transferred into the cryogenic STM immediately after film growth to minimize adsorption from the rest gas.

Theoretical insight into the MgO/Au(111) system was obtained from DFT calculations based on the projector-augmented wave method and a plane-wave basis set, as implemented in the Vienna *Ab initio* Simulation Package (VASP).[30,31] Results of the DFT–generalized gradient approximation (GGA; Perdew-Wang [PW] 91) approach were complemented by data obtained with the Heyd-Scuseria-Ernzerhof (HSE06) hybrid functional for the exchange correlation[32] and by incorporating van der Waals interactions via a semiempirical dispersion potential introduced by Grimme (DFT-D2).[32,33] The metal-oxide system was modeled with an asymmetric, five-layer gold slab having a bare and a MgO-covered surface, separated by 10 Å of vacuum. Spurious interactions between repeated dipoles were eliminated with conventional dipole-correction schemes. All MgO structures were fully relaxed until residual forces dropped below 0.01 eV/Å. Atomic charges were estimated within the Bader decomposition scheme.[34,35]

III. RESULTS AND DISCUSSION

A. Morphological and electronic properties of MgO islands in the STM

An STM topographic image of the Au(111) sample after MgO deposition is shown in Fig. 1(a). The surface is covered with triangular islands that lift the gold herringbone reconstruction beneath.[36] Two island orientations are distinguishable with one corner of the triangle either pointing down or up, i.e., along an Au$[\bar{1}\bar{1}2]$ or $[11\bar{2}]$ direction. The oxide triangles have rather uniform edge lengths of about 100 Å and are 2.5 Å in height, being compatible with a Mg-O monolayer. The island edges are parallel to the Au$[1\bar{1}0]$ directions and run along close-packed rows of the hexagonal MgO lattice [Fig. 1(b)]. Such configuration corresponds to zigzag-type edges that are terminated either by O or Mg rows, as depicted in the ball model of Fig. 2. The alternation of positive and negative ion rows along these edges induces an in-plane dipole moment, which diverges with increasing island size and can be considered as analogue to the out-of-plane polarity in films with alternating cationic and anionic planes.[25,27] The island top facet is not entirely flat but covered with a small number of 1 Å high protrusions [see height profile in Fig. 1(d)]. Similar maxima are found along the island edges and corners. Atomically resolved images, acquired at low sample bias (V_s), reveal a hexagonal atom arrangement of ~3.1 Å periodicity. This lattice symmetry indicates a (111) orientation of the

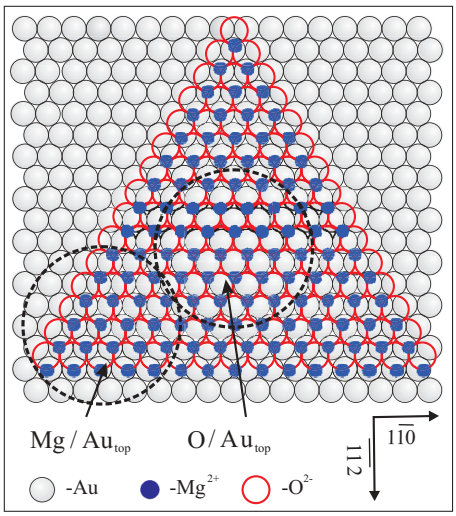

FIG. 2. (Color online) Ball model of a triangular MgO(111) island grown on Au(111). All oxide edges belong to the zigzag type. Note the change in registry when going from the island center to the edges due to lattice mismatch between oxide and metal support.

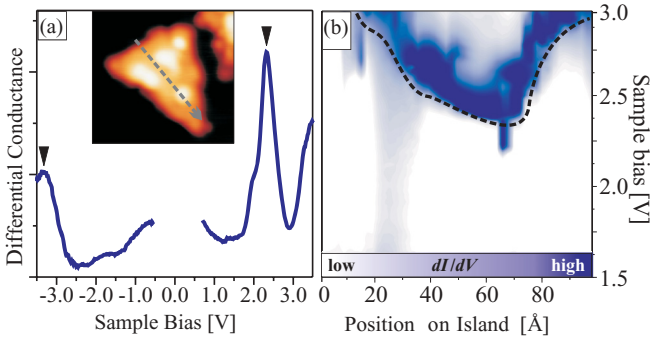

FIG. 3. (Color online) (a) dI/dV_s spectrum taken in the center of the triangular MgO island shown in the inset ($V_s = 0.5$ V, 100×100 Å^2). Two labels mark the valence and conduction-band onset. (b) Series of 100 dI/dV_s spectra taken along the line shown in the inset (a). The onset of the MgO conduction band, visualized by the broken line, varies considerably within the island. Particularly high onset energies are found at the island edges. Note the occurrence of low-bias electronic states at the island periphery at x positions of 25 and 100 Å.

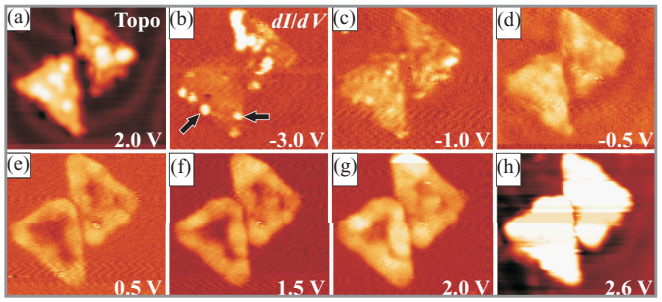

FIG. 4. (Color online) Topographic image and dI/dV_s maps of two triangular MgO islands on Au(111) taken as a function of sample bias (170×170 Å^2). Whereas localized states appear at the island edges at negative bias (b), the entire periphery turns bright at positive polarity (e)–(g). At 2.6 V, the MgO conduction band is reached, and the whole island appears with high contrast (h).

MgO with a lattice parameter that is 4% larger than the one of Au(111). The development of MgO(111) islands on the Au(111) support has been verified with low-energy electron and grazing incidence x-ray diffraction, both revealing two hexagonal spot patterns of similar size.[36] While the outer spots belong to the smaller Au(111) lattice, the inner ones reflect the slightly larger atom periodicity of the oxide film (not shown).

Insight into the electronic structure of the oxide islands is obtained from STM conductance spectra taken with enabled feedback loop. A wide-range spectrum measured in the center of a triangular island is shown in Fig. 3(a). The two maxima at -3.3 V and $+2.3$ V mark the onsets of the MgO valence and conduction band, respectively. The band gap of 5.6 eV is smaller than the MgO bulk value of 7.8 eV, reflecting the finite size of the island. The MgO(111) patches exhibit a n-type conductance characteristic, as the conduction band is much closer to the Au Fermi level than the valence band. To gain spatially resolved information on the band onsets, a spectral series has been taken across such a triangular island [Fig. 3(b)]. The individual dI/dV_s spectra are plotted as 2D matrix, with x and y axes marking the position on the island and the bias voltage, respectively, while the color encodes the dI/dV_s signal strength. In this representation, the MgO conduction band shows up as dark line, and the gap region appears white. The plot displays a concave shape of the band onset across the island with the highest and lowest values being located at the island edges and in the center, respectively. Discontinuities in this course, as noticeable at $x \sim 70$ Å, relate to instabilities in the tunnel current during spectral acquisition and typically occur for tip positions above the protrusions on the island top facet. A similar behavior was revealed for the valence band, suggesting a rigid shift of the MgO bands across the oxide island. Additional dI/dV_s features were detected along the island edges, where a weak signal occurs even inside the fundamental band gap [see light blue (light gray) region at $x \sim 25$ and $x \sim 100$ Å in Fig. 3(b)]. The associated electronic states are empty and cover a bias range from $+0.5$ V to the conduction band onset.

The spatial localization of the different spectral features becomes evident in bias-dependent dI/dV_s maps, as shown for two triangular MgO islands in Fig. 4(a). Above the valence-band onset at negative bias, bright dI/dV_s spots of $\sim$10 Å diameter appear along the island edges [see arrows in Fig. 4(b)]. They are detectable only in a small bias window, indicating the discrete nature of the underlying electronic states. A plausible explanation for these dI/dV_s maxima is electron tunneling out of filled states with high spatial localization, as produced by O or Mg defects at the island perimeter. Similar gap states have been observed for nonpolar MgO(001) films and were assigned to different O vacancies along the edges.[37] Only a faint dI/dV_s signal is detected at bias voltages within the MgO band gap, reflecting the absence of electronic states for tunneling [Figs. 4(c) and 4(d)]. The island perimeter is an exception, as it appears as a bright rim around the islands at positive sample bias [Figs. 4(e) and 4(f)]. This dI/dV_s enhancement reproduces the spectroscopy results shown in Fig. 3(b), where a weak conductance signal inside the fundamental gap was found along the edges as well. The associated electronic states are empty and extend over a wide bias range. At $+2.6$ V, the MgO conduction band and therewith an effective transport channel into the oxide patches is reached [Fig. 4(h)]. Consequently, the islands turn bright in the dI/dV_s maps, an effect that starts in the interior and proceeds to the outer regions with increasing bias. This gradual expansion of the high-conductance zone reflects the concave band shape in the MgO islands, a fact deduced already from the spectral series in Fig. 3(b).

Insight into the potential landscape above the MgO(111) triangles is finally obtained from STM barrier-height maps, which probe the effective tunnel barrier experienced by electrons on their way between tip and sample. Qualitatively, the barrier is larger for surface regions with high work function, however, no quantitative analysis can be made due to the unknown impact of the STM tip on the potential course. Barrier-height maps, acquired with the procedure introduced in Sec. II, are shown for a couple of MgO(111) patches in Fig. 5(a) and for a single island in 5(b). The Φ_{eff} signal is systematically lower above the oxide film than the Au(111) surface, indicating a higher work function of the bare metal. Moreover, the effective barrier height is not uniform inside the

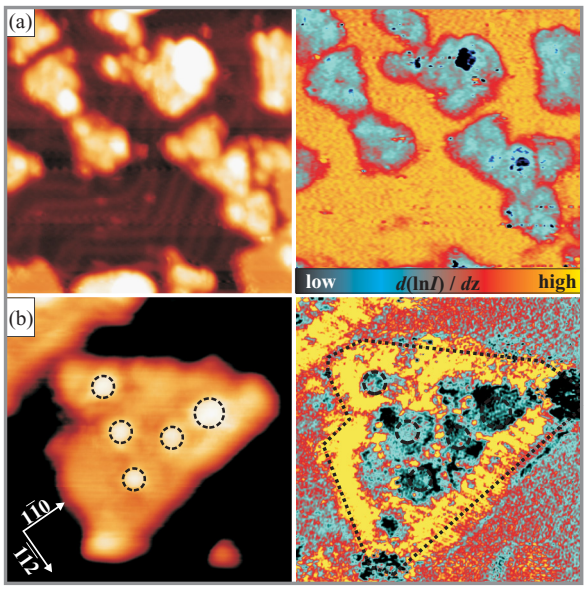

FIG. 5. (Color online) (a) Topographic and effective barrier-height (ϕ_{eff}) image of MgO islands on Au(111) ($V_s = -0.25$ V, 500×500 Å^2). The oxide systematically lowers the barrier-height signal with respect to the bare metal. (b) Topographic and ϕ_{eff} map of a single MgO island (90×90 Å^2). Note the enhanced barrier height at the island perimeter and the minima above the ad-structures in the center.

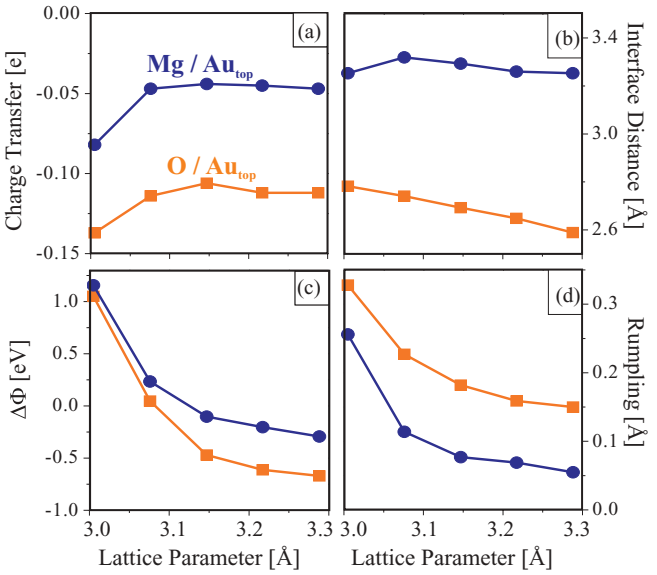

FIG. 6. (Color online) Structural and electronic properties of MgO(111)/Au(111) monolayer films with O/Au$_{\text{top}}$ and Mg/Au$_{\text{top}}$ registry, as function of the in-plane lattice parameter a: (a) charge transfer to the Au support, (b) interface distance, (c) MgO-induced change of the metal workfunction $\Delta\Phi$, and (d) film rumpling. A positive rumpling corresponds to an outward shift of the anions. All results are obtained at the DFT-GGA level, corresponding data from DFT-D2 and DFT-HSE06 are shown in the supplementary material (Ref. 38).

islands but features pronounced modulations. Particularly low Φ_{eff} values are detected above the protrusions on the island top facet, while larger values are measured at the edges, suggesting a work function increase at the perimeter. We will show in the next section that these modulations arise from structural as well as electrostatic effects in MgO(111) nanostructures.

B. Theoretical insight into the MgO(111) islands

To connect the experimental observations with structural and electronic properties of the MgO islands, we have simulated various (111)-oriented MgO monolayer structures on Au(111). In a first step, we have considered an infinite MgO film with the O ions sitting in Au-top adsorption sites (O/Au$_{\text{top}}$ registry). The lattice mismatch was accommodated by adapting the in-plane lattice parameter a of the Au support.[17] By comparing DFT-GGA(PW91), DFT-HSE06, and DFT-D2 calculations we verified that, regardless of the approach, the equilibrium lattice constant a is close to 3.3 Å, i.e., somewhat larger than the measured value of 3.1 Å. We therefore discuss structural and electronic properties for supported MgO(111) films with a values ranging from 3.0–3.3 Å in order to avoid any bias due to the choice of a particular a (Fig. 6).

All results presented here can be explained by considering the charge transfer across the metal-oxide interface and the subsequent distortion of the oxide lattice, in agreement with the induced polar character of the MgO films.[17,18] In sharp contrast to a bulk rocksalt structure, MgO(111) monolayers are nearly planar and lose electrons to the electronegative gold support [Fig. 6(a)]. The extra charges in the metal repel the oxide anions and attract the cations, inducing an outward relaxation of the O plane and hence a positive rumpling of the film [Fig. 6(d)]. The dipole moment associated with this rumpling stands opposite to the induced dipole due to the interface charge transfer.[17] Two regimes are distinguishable as a function of the lattice parameter. For $a > 3.1$ Å, the film rumpling is small, and the dipoles due to interfacial charge transfer and film rumpling compensate each other.[17] This situation gives rise to a negative work function change ($\Delta\Phi < 0$) with respect to pure Au(111) that can be rationalized with the compression of the electron-dipole layer on the gold surface by the oxide film [Fig. 6(c)]. On bare metals, the spill-out of the electron gas largely contributes to the work function, an effect that vanishes on MgO-covered surfaces as the Pauli repulsion of the oxide ions pushes the electron density back into the metal.[19] With decreasing lattice parameter, the film rumpling increases due to increasing steric repulsion between anions and cations. Eventually, the associated rumpling dipole overrides all other electrostatic contributions, as it cannot be balanced any more by a larger interface charge transfer. As a result, $\Delta\Phi$ becomes positive and the MgO bands shift to higher energy (Fig. 7).

The experimental in-plane lattice parameter of MgO(111) islands, $a = 3.1$ Å, is now at the borderline between the two regimes. The real films are therefore expected to develop a sizeable rumpling of 0.1–0.2 Å, although the effect is too small to turn $\Delta\Phi$ positive. The MgO(111) monolayer thus lowers the Au(111) work function, in agreement with the reduction of the barrier-height level in the STM measurements (Fig. 5). In the supplementary material,[38] we show that this is a robust finding that can be reproduced with all computational approaches considered here.

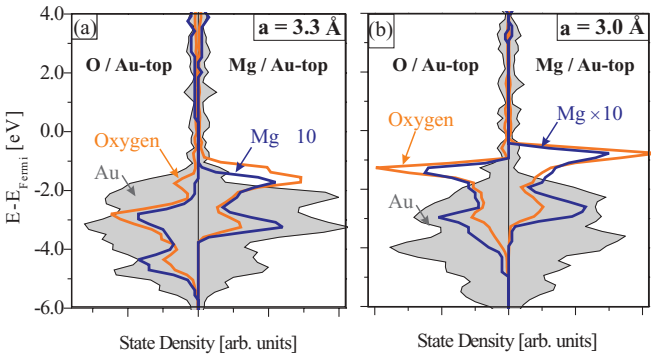

FIG. 7. (Color online) Density of states projected onto Mg (blue/gray) and O (orange/dark gray) ions calculated for (a) a lattice parameter of 3.3 Å and (b) of 3.0 Å. Calculations are performed on the DFT-GGA level, corresponding data from the DFT-HSE06 approach are shown in the supplementary material (Ref. 38).

The most interesting experimental outcome is, however, the deviating electronic properties in the center and along the perimeter of the MgO(111) islands. Possible structural and electronic effects that may contribute to this difference are discussed in the following.

(a) Lattice registry. Due to the mismatch in the MgO(111) and the unreconstructed Au(111) lattice parameter, the energetically favorable O/Au_{top} registry cannot be realized in the whole island but deteriorates when moving from the center towards the edges. At the periphery, the atomic configuration likely approaches the unfavorable Mg/Au_{top} registry that finally suppresses the island expansion [Fig. 1(a)].[27] To mimic the resulting interface structure we have modeled an infinite MgO film in which the Mg ions bind to the Au atoms (Mg/Au_{top} registry). This interface registry is less stable by 0.2 eV (DFT-GGA and DFT-HSE06) and 0.3 eV per MgO unit cell (DFT-D2) than the preferred O/Au_{top} configuration. Moreover, the metal-oxide binding length is larger for the Mg/Au_{top} registry [Fig. 6(b)], which gives rise to a smaller interface charge transfer [Fig. 6(a)] and a smaller rumpling of the MgO film [Fig. 6(d)]. The wider interface partly restores the effect of electron spill out at the Au surface and leads to a work function rise. The change in lattice registry also alters the MgO band alignment. When moving from the O/Au_{top} to the Mg/Au_{top} configuration, the bands are pushed to higher energy in response to the increased electron density at the wider interface [Figs. 7(a)]. The modified lattice registry upon approaching the island edges thus leads to an upshift of the band edges and to a rise in the work function, reproducing the concave band shape [Fig. 3(b)] and the enhanced tunneling barrier at the island perimeter [Fig. 5(b)] found experimentally.

(b) Edge effects. The STM data suggest that edges around the oxide triangles are of zigzag type, i.e., terminated by either close-packed O or Mg rows running along an Au[$1\bar{1}0$] direction.[27] This edge orientation is polar and requires compensating charges to be stabilized. In absence of charged adsorbates and nonstoichiometric edge compositions, the compensating charges may be provided by edge metallization and the gold support. To model the impact of polar edges on the local electronic structure, we have considered an infinite MgO(111) stripe (seven MgO units wide) delimited by an Mg- and an O-terminated zigzag edge. Following our earlier discussion, we have chosen the Mg/Au_{top} lattice registry that is typical for the island edges. Figure 8(a) shows a map of the electrostatic energy above such as an MgO stripe, with more negative values corresponding to more negative work function changes $\Delta\Phi$. Whereas the overall potential varies only little when going from the MgO stripe to the Au support, reflecting the small $\Delta\Phi$ shift for the Mg/Au_{top} configuration [Fig. 6(c)], a distinct pattern becomes visible at the Mg edge. It arises from an outward relaxation of the oxide ions by 1.4 Å, induced by the strong Au-Mg bonding directly at the Mg edge and the accumulation of compensating electrons in the Au surface beneath. At the O-terminated edge, the reverse compensation mechanism takes place, which has, however, a smaller effect on structure and electrostatic potential of the stripe. In general, the edge-induced potential modulations are of the order of 0.25 eV and thus smaller than the $\Delta\Phi$ changes induced by the registry switch between island center and periphery (0.5 eV).

(c) Edge hydroxylation. We have shown that the in-plane polarity induced by zigzag edges can effectively be quenched with charged ad-species, e.g., OH groups.[27] In the experiments, small amounts of water in the rest gas may therefore spontaneously dissociate and produce a sizeable stabilization of the MgO edges. We have modeled this effect by adding H and OH groups to the O- and Mg-terminated edges of the MgO stripe, respectively, and find indeed substantial effects on its structure and potential landscape [Fig. 8(b)]. As the edge polarity is quenched upon hydroxylation, the Au substrate no longer provides compensating charges, and the outward relaxation of ions at the Mg edge vanishes. Conversely, the density of states along the edges is significantly altered by the adsorbed OH groups. While bands at the O edge experience a down shift with respect to the stripe center, their position remains unchanged at the Mg edge [Fig. 8(b), lower panel]. This difference reflects the higher coordination of OH groups at the O edge (twofold) compared to their terminal geometry at Mg edges. Again, the potential modulations due to edge hydroxylation are small compared to those induced by changes in the lattice registry.

Finally, we have looked at hydrogenation effects in the central part of the island. For this purpose, we used a stripe with O/Au_{top} registry, representative for the island center, and attached a row of H-atoms in the middle [Fig. 8(c)]. The adsorption causes the respective OH groups to relax outward by almost 0.5 Å, which in turn leads to a downshift of about 1 eV of both the local surface potential and the oxide bands. It is worth noting that the enhanced film rumpling in this case is accompanied by a reduction of the in-plane lattice parameter.

C. Discussion

As a first important result of our study, we conclude that the properties of the MgO(111) islands are incompatible with an as-cut rocksalt structure.[36] Despite the undercoordination of the ions, the measured in-plane lattice parameter is considerably larger than the bulk value. This in-plane expansion is consistent with the nearly flat MgO(111) film found in the calculations, the rumpling of which is one order of magnitude smaller than the layer distance in bulk MgO(111). Note that the

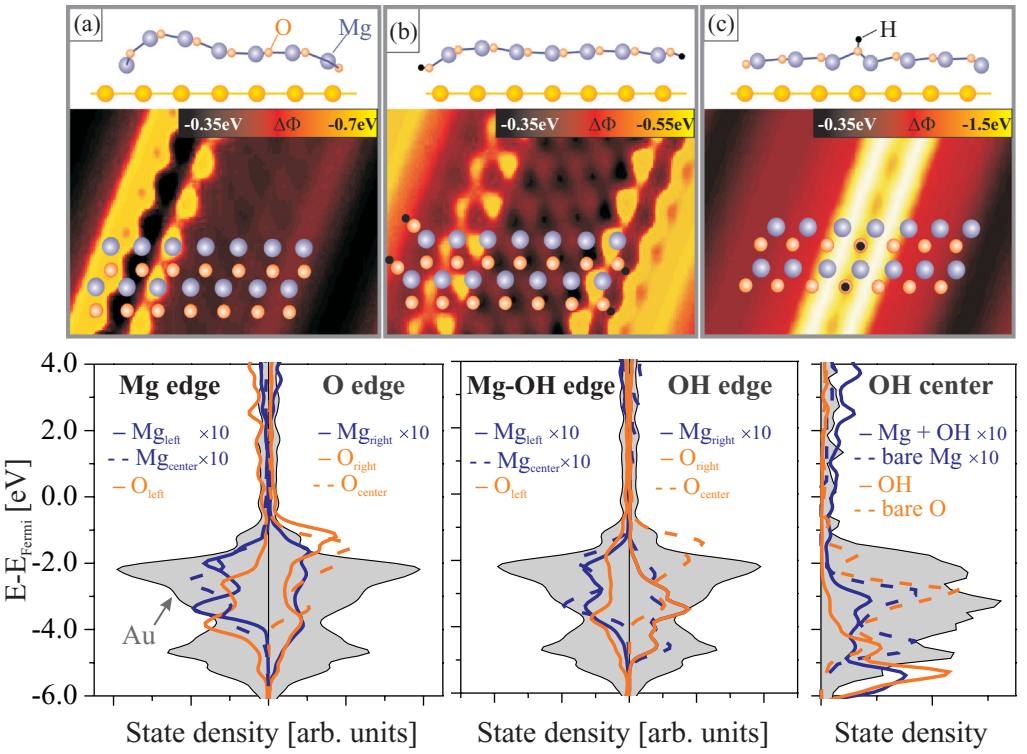

FIG. 8. (Color online) Maps of the electrostatic potential taken 7 Å above an Au-supported MgO(111) stripe terminated with zigzag edges. The MgO lattice parameter a was set to 3.3 Å. Lateral positions of the Mg and O ions are indicated with large blue and small red circles, respectively; vertical positions are shown in the top panels: (a) bare stripe, (b) hydroxylated stripe, and (c) stripe with a hydrogen row in the middle. The lower panels display the respective LDOS projected onto different Mg and O ions on the Mg- (left) and O-terminated edge (right) as calculated at the DFT-GGA level.

rumpling is not a remnant of the rocksalt structure but reflects the response of the dielectric film to the interface electron transfer, as subsumed by the term 'induced polarity'.[17,18] The calculations also disclosed the origin of the observed increase in band energy and barrier height when moving from the center to the periphery of the MgO(111) islands. The largest impact on $\Delta\Phi$ comes from the interface registry that changes from the preferred O/Au_{top} in the center to the unfavorable Mg/Au_{top} at the island edges. This shift leads to a gradual increase of the metal-oxide binding length, accompanied by a work function rise due to enhanced electron spill out at the interface. Other effects, such as the lower coordination of the edge atoms, the polarization of the metal beneath, and possible hydroxylation effects are of minor importance for the phenomena detected in STM. A more subtle electronic effect concerns the edge-electronic states that govern the dI/dV_s maps taken inside the band gap and give rise to the rim around the oxide islands (Fig. 4). Our simulations suggest two reasons for the occurrence of such empty-edge states. The first one is Mg-Au hybridization along the dry Mg-terminated edges, which results in an enhanced Mg-derived state density in the band gap [see Fig. 8(a)]. The second one relates to hydroxylation of the O edges that again leads to a higher state density in the gap region [Fig. 8(b)]. Local hydroxylation via the rest gas might also produce the small ad-features that cover the top of the triangular MgO(111) islands [Fig. 5(b)]. Our calculations showed that already a few terrace OH groups might induce a considerable downshift of the local surface potential, in line with the findings of the barrier-height maps. Note that also nonstoichiometric MgO nanopyramids, constituting the building blocks of the octopolar reconstruction on bulk MgO(111), might be responsible for the observed barrier-height modulations across the islands. However, the instability of the ad-features during scanning supports an assignment to surface OH-groups.

Let us emphasize that the spectroscopic data obtained on MgO(111) nanoislands leaves room for alternative interpretations. Polarity compensation at the edges might also be achieved by nonstoichiometric edge compositions, being inaccessible to our experimental approach. This option becomes particularly relevant as the role of hydroxylation is not exactly known, and earlier x-ray photoelectron spectra only provided a rough estimation of the OH amount (∼5%).[36] Moreover, the STM results may not represent the initial MgO configuration, as hydrogen is known to desorb upon electron injection from the STM tip.[39,40] Despite these experimental uncertainties, we are confident that changes in the lattice registry dominate the electronic properties of the MgO(111) islands, while other effects (edge termination, hydroxylation, etc.) are less relevant.

IV. CONCLUSION

STM conductance and barrier-height measurements revealed an inhomogeneous electronic structure and a modulated potential landscape for monolayer MgO(111) islands grown

on Au(111). The oxide bands exhibit a concave shape across the islands with the highest and lowest positions found at the periphery and in the center, respectively. Also, the surface potential reaches particularly high values at the island edges with respect to the inner parts. DFT calculations on different MgO(111) model structures identified the reasons for this behavior. The monolayer oxide exhibits an interlayer distance that is much smaller than in bulk MgO(111), providing evidence for the induced-polar character of the oxide film. The largest impact on the local electronic structure comes from a change in lattice registry when moving from the island center to the periphery, reflecting the lattice mismatch between MgO(111) and Au(111). The polar nature of the island edges, on the other hand, is only of minor importance, in correspondence with the effective polarity compensation via the gold substrate.

Our work visualizes the complex interplay between structural and electrostatic phenomena occurring on spatially confined ionic systems. Especially along the periphery, a number of unusual effects were found, e.g., residual edge polarity, band shifts, and low-lying electronic states. Such electronic perturbations will determine the edge reactivity and hence the chemical properties of the entire nanostructure. While the MgO(111)/Au(111) system is mainly of academic interest in this regard, the generic phenomena discussed here will occur at any metal-oxide interface and thus control the functionality of supported-metal catalysts and microelectronic devices.

ACKNOWLEDGMENTS

The experimental work has been supported by the DFG excellence initiative 'UNICAT' (N.N. and Y.P.) and the Italian MIUR through the FIRB Project RBAP115AYN (S.B.). J.G. and C.N. gratefully acknowledge the generous allocation of computing time on the IBM Power 6 cluster at IDRIS under Project No. 100170. We thank Gianfranco Pacchioni and Hans-Joachim Freund for helpful discussions.

*Corresponding authors: nilius@fhi-berlin.mpg.de; jacek.goniakowski@insp.jussieu.fr

[1] J. Goniakowski, F. Finocchi, and C. Noguera, Rep. Prog. Phys. **71**, 016501 (2008).
[2] H.-J. Freund and G. Pacchioni, Chem. Soc. Rev. **37**, 2224 (2008).
[3] N. Nilius, Surf. Sci. Rep. **64**, 595 (2009).
[4] F. P. Netzer, F. Allegretti, and S. Surnev, J. Vac. Sci. Technol. B **28**, 1 (2010).
[5] Q. H. Wu, A. Fortunelli, and G. Granozzi, Int. Rev. Phys. Chem. **28**, 517 (2009).
[6] M. Kiguchi, S. Entani, K. Saiki, T. Goto, and A. Koma, Phys. Rev. B **68**, 115402 (2003).
[7] G. H. Vurens, M. Salmeron, and G. A. Somorjai, Surf. Sci. **201**, 129 (1988).
[8] M. Ritter, W. Ranke, and W. Weiss, Phys. Rev. B **57**, 7240 (1998).
[9] E. D. L. Rienks, N. Nilius, H.-P. Rust, and H.-J. Freund, Phys. Rev. B **71**, 241404 (2005).
[10] G. Weirum, G. Barcaro, A. Fortunelli, F. Weber, R. Schennach, S. Surnev, and F. P. Netzer, J. Phys. Chem. C **114**, 15432 (2010).
[11] J. Goniakowski, C. Noguera, and L. Giordano, Phys. Rev. Lett. **98**, 205701 (2007).
[12] J. Goniakowski, C. Noguera, and L. Giordano, Phys. Rev. Lett. **93**, 215702 (2004).
[13] C. Tusche, H. L. Meyerheim, and J. Kirschner, Phys. Rev. Lett. **99**, 026102 (2007).
[14] L. Gragnaniello, G. Barcaro, L. Sementa, F. Allegretti, G. Parteder, S. Surnev, W. Steurer, A. Fortunelli, and F. P. Netzer, J. Chem. Phys. **134**, 184706 (2011).
[15] L. Giordano, G. Pacchioni, J. Goniakowski, N. Nilius, E. D. L. Rienks, and H.-J. Freund, Phys. Rev. B **76**, 075416 (2007).
[16] C. L. Freeman, F. Claeyssens, N. L. Allan, and J. H. Harding, Phys. Rev. Lett. **96**, 066102 (2006).
[17] J. Goniakowski and C. Noguera, Phys. Rev. B **79**, 155433 (2009).
[18] J. Goniakowski, L. Giordano, and C. Noguera, Phys. Rev. B **81**, 205404 (2010).
[19] L. Giordano, F. Cinquini, and G. Pacchioni, Phys. Rev. B **73**, 045414 (2006).
[20] T. König, G. H. Simon, H. P. Rust, and M. Heyde, J. Phys. Chem. C **113**, 11301 (2009).
[21] Y. Pan, S. Benedetti, N. Nilius, and H.-J. Freund, Phys. Rev. B **84**, 075456 (2011).
[22] H. M. Benia, P. Myrach, N. Nilius, and H.-J. Freund, Surf. Sci. **604**, 435 (2010).
[23] S. Benedetti, F. Stavale, S. Valeri, C. Noguera, H.-J. Freund, J. Goniakowski, and N. Nilius, Adv. Funct. Mater. (2012), doi: 10.1002/adfm.201201502.
[24] E. D. L. Rienks, N. Nilius, H.-P. Rust, and H.-J. Freund, Phys. Rev. B **71**, 241404 (2005).
[25] J. Goniakowski and C. Noguera, Phys. Rev. B **83**, 115413 (2011).
[26] M. V. Bollinger, J. V. Lauritsen, K. W. Jacobsen, J. K. Nørskov, S. Helveg, and F. Besenbacher, Phys. Rev. Lett. **87**, 196803 (2001).
[27] Y. Pan, S. Benedetti, S. Valeri, C. Noguera, L. Giordano, J. Goniakowski, and N. Nilius, J. Phys. Chem. C **116**, 11126 (2012).
[28] J. C. Chen, *Introduction to Scanning Tunneling Microscopy* (Oxford University Press, New York, 1993).
[29] L. Olesen, M. Brandbyge, M. R. Sorensen, K. W. Jacobsen, E. Laegsgaard, I. Stensgaard, and F. Besenbacher, Phys. Rev. Lett. **76**, 1485 (1996).
[30] J. P. Perdew and Y. Wang, Phys. Rev. B **45**, 13244 (1992); D. Vanderbilt, *ibid.* **41**, 7892 (1990).
[31] G. Kresse and J. Hafner, Phys. Rev. B **47**, 558 (1993); G. Kresse and J. Furthmüller, *ibid.* **54**, 11169 (1996).
[32] J. Heyd, G. E. Scuseria, and M. Ernzerhof, J. Chem. Phys. **124**, 219906 (2006).
[33] S. Grimme, J. Comput. Chem. **27**, 1787 (2006).
[34] R. F. W. Bader, Chem. Rev. **91**, 893 (1991).
[35] G. Henkelman, A. Arnaldsson, and H. Jonsson, Comput. Mater. Sci. **36**, 354 (2006); W. Tang, E. Sanville, and G. Henkelman, J. Phys.: Condens. Matter **21**, 084204 (2009).
[36] S. Benedetti, N. Nilius, P. Torelli, G. Renaud, H.-J. Freund, and S. Valeri, J. Phys. Chem. C **115**, 23043 (2011).

[37]M. Sterrer, M. Heyde, M. Nowicki, N. Nilius, T. Risse, H.-P. Rust, G. Pacchioni, and H.-J. Freund, J. Phys. Chem. B **110**, 46 (2006).

[38]See Supplemental Material at http://link.aps.org/supplemental/10.1103/PhysRevB.86.205410 for a comparison of the theoretical description of supported MgO(111) islands using different computational approaches that are standard DFT-GGA (PW91), DFT-D2 (PW91), and DFT-HSE06 (PBE).

[39]T. Hitosugi, T. Hashizume, S. Heike, S. Watanabe, Y. Wada, T. Hasegawa, and K. Kitazawa, Jpn. J. Appl. Phys. **36**, L361 (1997).

[40]E. T. Foley, A. F. Kam, J. W. Lyding, and P. Avouris, Phys. Rev. Let. **80**, 1336 (1998).